Supplementary Information

Figure S1. LPA treatment prevents starvation-induced ciliogenesis and Rabin8 trafficking, related to Figure 1.

(A) Representative plot (mean ± s.d.) of cell cycle analysis performed as described in Fig 1B for treatments in Fig 1A from two independent experiments. $P < 0.001$ (***) for G_0/G_1 are shown. (B, C) Quantification of ciliation (B) from immunostained RPE-1 cells (C) treated with serum, starved for 24h, or starved for 24h in the presence of LPA. Cells were stained with acetylated a-tubulin (^{Ac}tub) and pericentrin antibodies. Scale bar = 10µm. (D) Representative plot (mean ± s.d.) of cell counts determined following 24h treatments described in Fig 1A and Fig 2E from two independent experiments. $P < 0.01$ (**) are shown. (E-H) Quantification of primary cilia in HPNE, MCF12, MEFs, and IMCD3 cells upon treatment with LPA (5µM) stained with acetylated a-tubulin (^{Ac}tub) and pericentrin antibodies. (I) Live-cell epifluorescence imaging showing GFP-Rabin8 association with tRFP-Rab11a vesicles within minutes of serum starvation in stably-expressing RPE-1 cells. Scale bar = 5µm. (J) RPE-1 GFP-Rab11a cells were treated with serum (2%), serum starved for 1h, and serum starved with LPA (5µM) for 1h and then fixed with PFA and stained with the MC marker CEP164 and DAPI. Scale bar = 10µm.

Figure S2. LPA regulates ciliogenesis through the LPAR1 receptor, related to Figure 2.

(A) Quantification of primary cilia in parental RPE-1 cells and RPE-1 LPAR1-GFP cells in serum and upon 24h starvation showing that cells overexpressing LPAR1-GFP ciliate upon serum starvation. Cells were stained with acetylated a-tubulin (^{Ac}tub) and pericentrin

antibodies. Mean ± s.d. is shown for n > 100 cells counted (B). Representative plot (mean ± s.d.) of cell cycle analysis performed as described in Fig 1B for the treatments in Fig 2D from two independent experiments. P <0.001 (***) for G_0/G_1 are shown for n>50 cells per treatment. (C) A dose-course effect of Ki16425 on RPE-1 cell ciliation in the presence of 2% FBS. Cells were stained as described in (A). (D) A dose-course effect of Ki16425 on RPE-1 cell ciliation in the presence of LPA (10μM). Cells were stained as described in (A). (E) Representative images from (D). Scale bar 10μm. (F, G) Representative plot (mean ± s.d.) of cell counts determined following 24h (F) and 1h treatments (G) with and without Ki16425 (10μM) as described in Fig S1D. (F) and Fig 2H (G) from two independent experiments. $P < 0.01$ (**) are shown.

Figure S3. Akt signaling and ciliogenesis, related to Figure 3.

(A) Quantification of Akt inhibitor MK-2206 (2.5 μM) effects on ciliogenesis as described in Figure S1B. Representative plot from two independent experiments with n>65 cells counted. Mean ± s.d. are shown. **$P < 0.01$. (B) Representative plot (mean ± s.d.) of cell counts determined following 24h treatments with MK-2206 as described in (A) from two independent experiments. $P < 0.01$ (**) are shown. (C) Representative plot (mean ± s.d.) of cell cycle analysis performed as described in Fig 1B on cells treated for 24h with MK-2206 as described in (A) two independent experiments. P <0.001 (***) for G_0/G_1 are shown. (D) RPE-1 cells were treated with EGF without serum for 24h and following 24h serum starvation for 5 (5') and 15 (15') minutes. Western analysis of cell lysate immunoblotted with $pAKT^{S473}$ and Akt antibodies. (E) Representative plot (mean ± s.d.) of cell cycle analysis performed on cells treated with siControl and sipanAkt for 72h as

described in Fig 3G from two independent experiments. P <0.001 (***) for G_0/G_1 are shown.

Figure S4. Akt phosphorylation sites at Ser147 and Ser149 of Rabin8 are not required to bind Rab11aQ70L or Rab8aT22N, related to Figure 4.

(A) Immunoprecipitation analysis of HA-Rab11aQ70L with wild-type, phosphomimetic (S147D/S149D), and phosphoinactive (S147A/S149A) mutants of GFP-Rabin8 expressed in 293T cells. Immunoblots were probed with GFP and HA antibodies. Blots shown are from the same experiment and exposure and are representative from two independent experiments. (B) Rabin8 fragment map. (C) Co-immunoprecipitation analysis of HA-Rab11aQ70L with GFP-Rabin8 fragments expressed as described in (A). Representative blot from two independent experiments is shown. (D) Co-immunoprecipitation analysis of HA-Rab8aT22N with WT, phosphomimetic, and phosphoinactive mutants of GFP-Rabin8 as described in (A). Blots shown are from the same experiment and exposure and are representative from two independent experiments. (E) Co-immunoprecipitation analysis of HA-Rab8T22N with GFP-Rabin8 fragments as described in (A). Representative blot from two independent experiments is shown.

Figure S5. WDR44 specifically binds Rab11 in a GTP-dependent manner, related to Figure 5.

(A) Coomassie staining of Rab11-binding proteins immunoprecipitated from stable GFP-Rab11a RPE-1 cell lysate. Cells were grown to 70% confluency in serum (+) and were serum-starved for 1h (-). (B, C) Co-immunoprecipitation of HA-WDR44 or FLAG-Rab11b

with GFP-Rab proteins transiently-expressed in 293T cells. (D) Representative plot (mean ± s.d.) of cell counts determined for siControl and siWDR44 72h treatments as described in Fig 5E from two independent experiments. $P < 0.01$ (**) are shown. (E) Representative plot (mean ± s.d.) of cell cycle analysis performed as described in Fig 1B on cells treated as described in (D) from two independent experiments. $P < 0.001$ (***) for G_0/G_1 are shown.

Figure S6. WDR44 phosphomutant binding to Rab11 and effects on Zebrafish KV formation, related to Figure 6.

(A) Immunoprecipitation showing binding of GFP-WDR44 wild-type, phosphomimetic (Aspartic acid), and phosphoinactive (Alanine) mutants (corresponding to the mapped Akt phosphorylation sites) with HA-Rab11aQ70L and immunoblotted with GFP and HA antibodies. Blots shown are from the same experiment and exposure. Representative western blots from three independent experiments is shown. (B) Analysis of Kupffer's vesicles (KV) from live embryos injected with WDR44 mutants and Rab11aS25N. Mean ± s.e.m from n>50 KVs analyzed from three independent experiments is shown. **P<0.001.

Figure S7. WDR44 binds to Rab11 with similar affinity as FIP3-Rab11 and competes with FIP3 for Rab11, related to Figure 7.

(A) Isothermal titration calorimetry experiment showing that the Rab11-WDR44 complex has a K_D of 0.54 ± 0.04μM. (B) Immunoprecipitation experiment showing that WDR44-Rab11 interaction could be inhibited by FIP3. HA-Rab11aQ70L was co-expressed with

untagged WDR44 and FIP3. RPE-1 cells were lysed, and cell lysates were immunoprecipitated with magnetic HA beads. (C) Isothermal titration calorimetry experiment titrating Rabin8C with a preformed Rab11aQL$_{6-186}$-WDR44$_{334-435}$ complex. Rabin8 affinity for Rab11-WDR44 is 37.2 ± 9.7 μM.

Figure S1

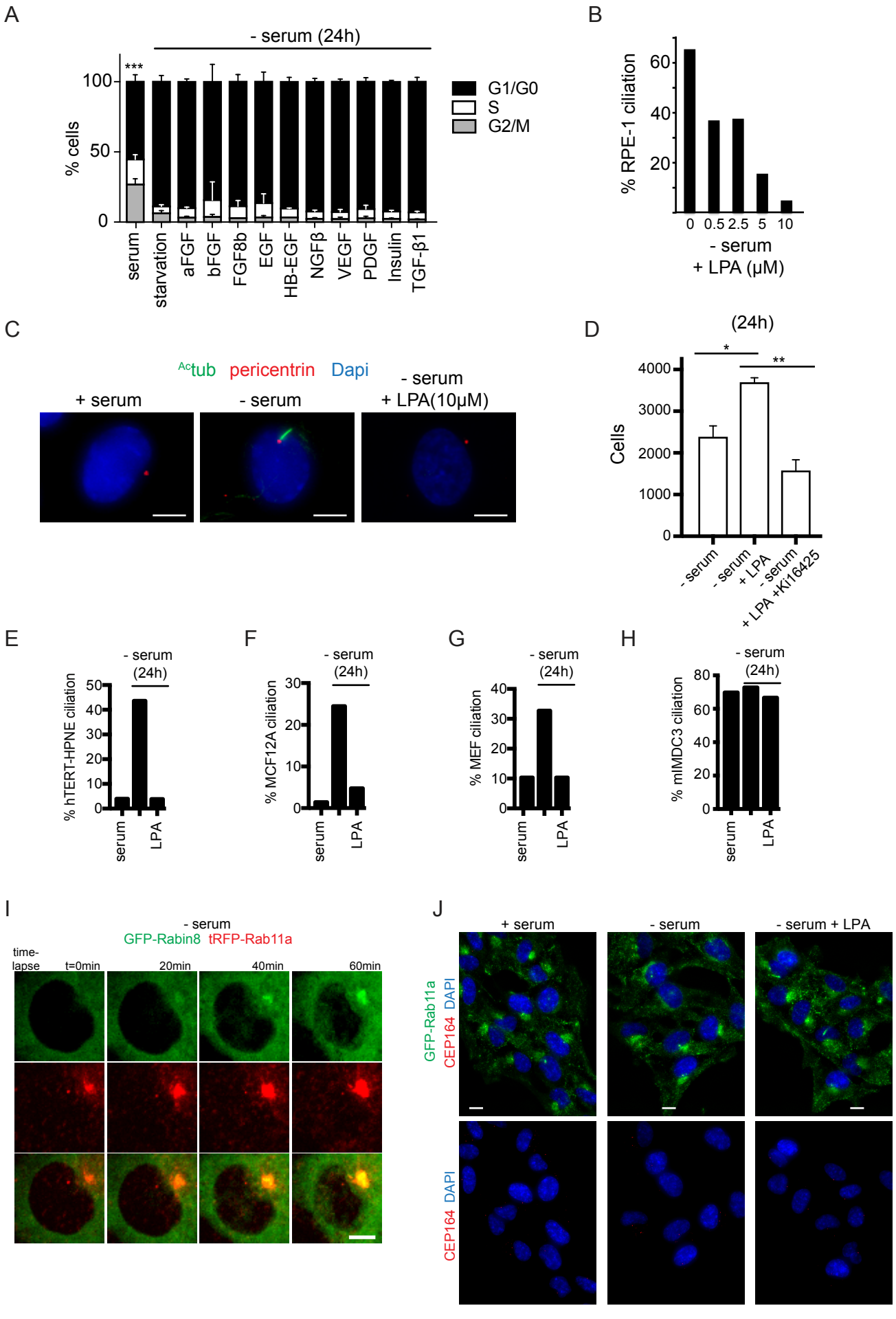
A
- serum (24h)
***
100
50
0
% cells
G1/G0
S
G2/M
serum
starvation
aFGF
bFGF
FGF8b
EGF
HB-EGF
NGFβ
VEGF
PDGF
Insulin
TGF-β1
B
% RPE-1 ciliation
60
40
20
0 0.5 2.5 5 10
- serum
+ LPA (μM)
C
Actub pericentrin Dapi
+ serum
- serum
- serum
+ LPA(10μM)
D
(24h)
*
**
4000
3000
2000
1000
0
Cells
- serum
- serum
+ LPA
- serum
+ LPA +Ki16425
E
- serum
(24h)
% hTERT-HPNE ciliation
50
40
30
20
10
0
serum
LPA
F
- serum
(24h)
% MCF12A ciliation
30
20
10
0
serum
LPA
G
- serum
(24h)
% MEF ciliation
40
30
20
10
0
serum
LPA
H
- serum
(24h)
% mIMDC3 ciliation
80
60
40
20
0
serum
LPA
I
- serum
GFP-Rabin8 tRFP-Rab11a
time-
lapse
t=0min
20min
40min
60min
J
+ serum
- serum
- serum + LPA
GFP-Rab11a CEP164 DAPI
CEP164 DAPI

Figure S2

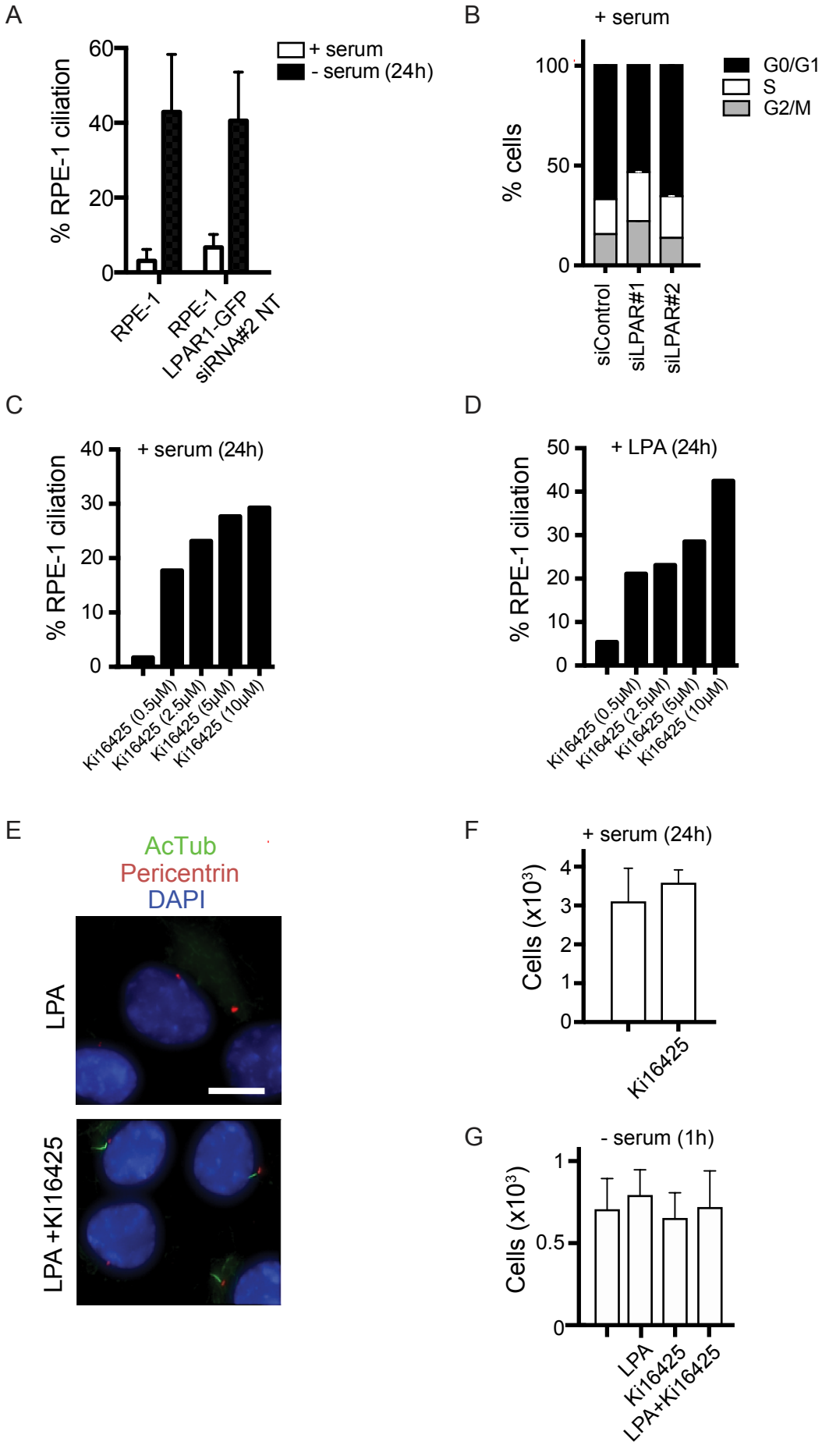
A
% RPE-1 ciliation
60
40
20
0
+ serum
- serum (24h)
RPE-1
RPE-1 LPAR1-GFP siRNA#2 NT
B
+ serum
100
50
0
% cells
G0/G1
S
G2/M
siControl
siLPAR#1
siLPAR#2
C
+ serum (24h)
% RPE-1 ciliation
40
30
20
10
0
Ki16425 (0.5μM)
Ki16425 (2.5μM)
Ki16425 (5μM)
Ki16425 (10μM)
D
+ LPA (24h)
% RPE-1 ciliation
50
40
30
20
10
0
Ki16425 (0.5μM)
Ki16425 (2.5μM)
Ki16425 (5μM)
Ki16425 (10μM)
E
AcTub
Pericentrin
DAPI
LPA
LPA +KI16425
F
+ serum (24h)
Cells (x10³)
4
3
2
1
0
Ki16425
G
- serum (1h)
Cells (x10³)
1
0.5
0
LPA
Ki16425
LPA+Ki16425

Figure S3

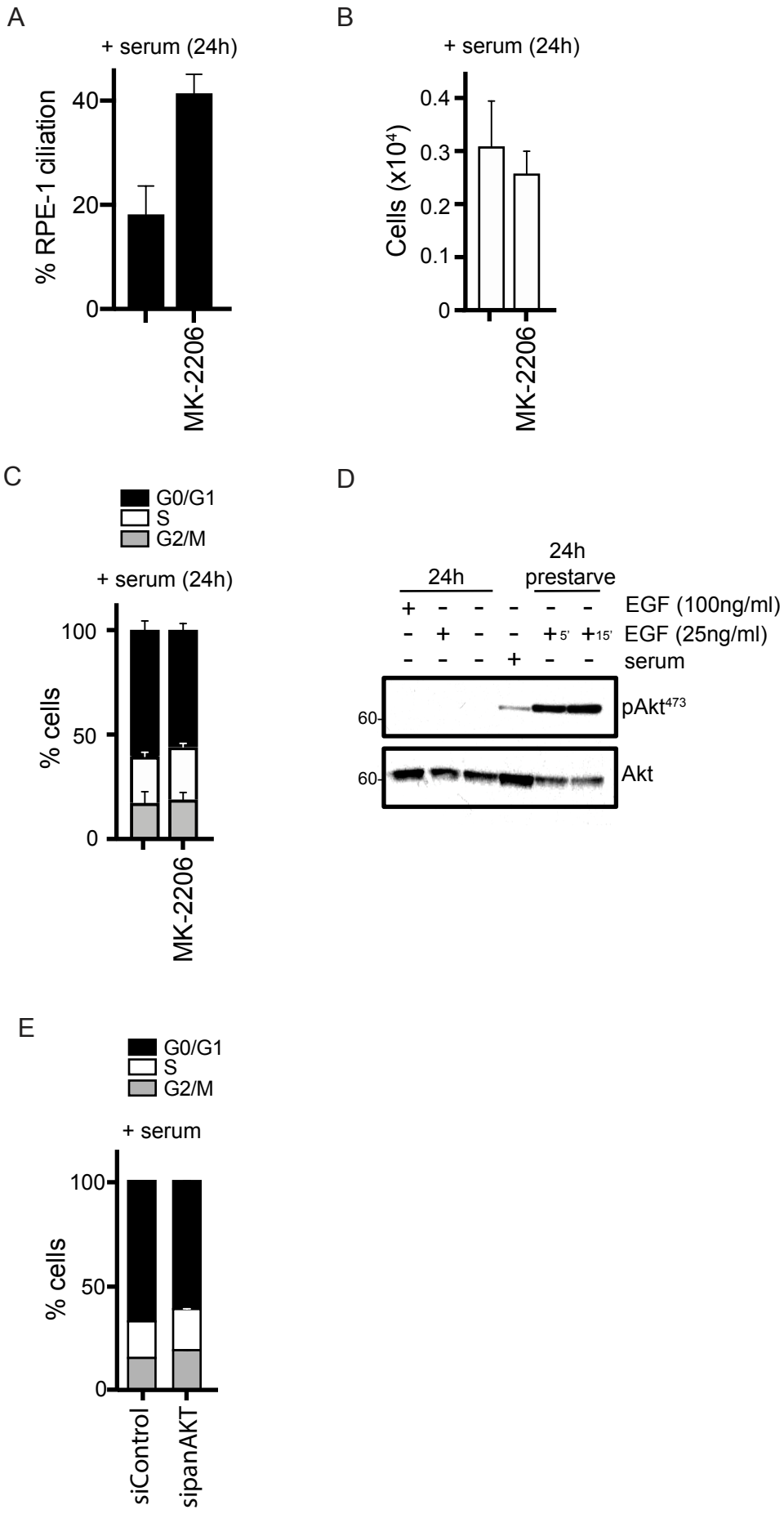
A
+ serum (24h)
% RPE-1 ciliation
40
20
0
MK-2206
B
+ serum (24h)
Cells (x10⁴)
0.4
0.3
0.2
0.1
0
MK-2206
C
G0/G1
S
G2/M
+ serum (24h)
% cells
100
50
0
MK-2206
D
24h
24h prestarve
EGF (100ng/ml)
EGF (25ng/ml)
serum
pAkt473
Akt
60
60
E
G0/G1
S
G2/M
+ serum
% cells
100
50
0
siControl
sipanAKT

Figure S4

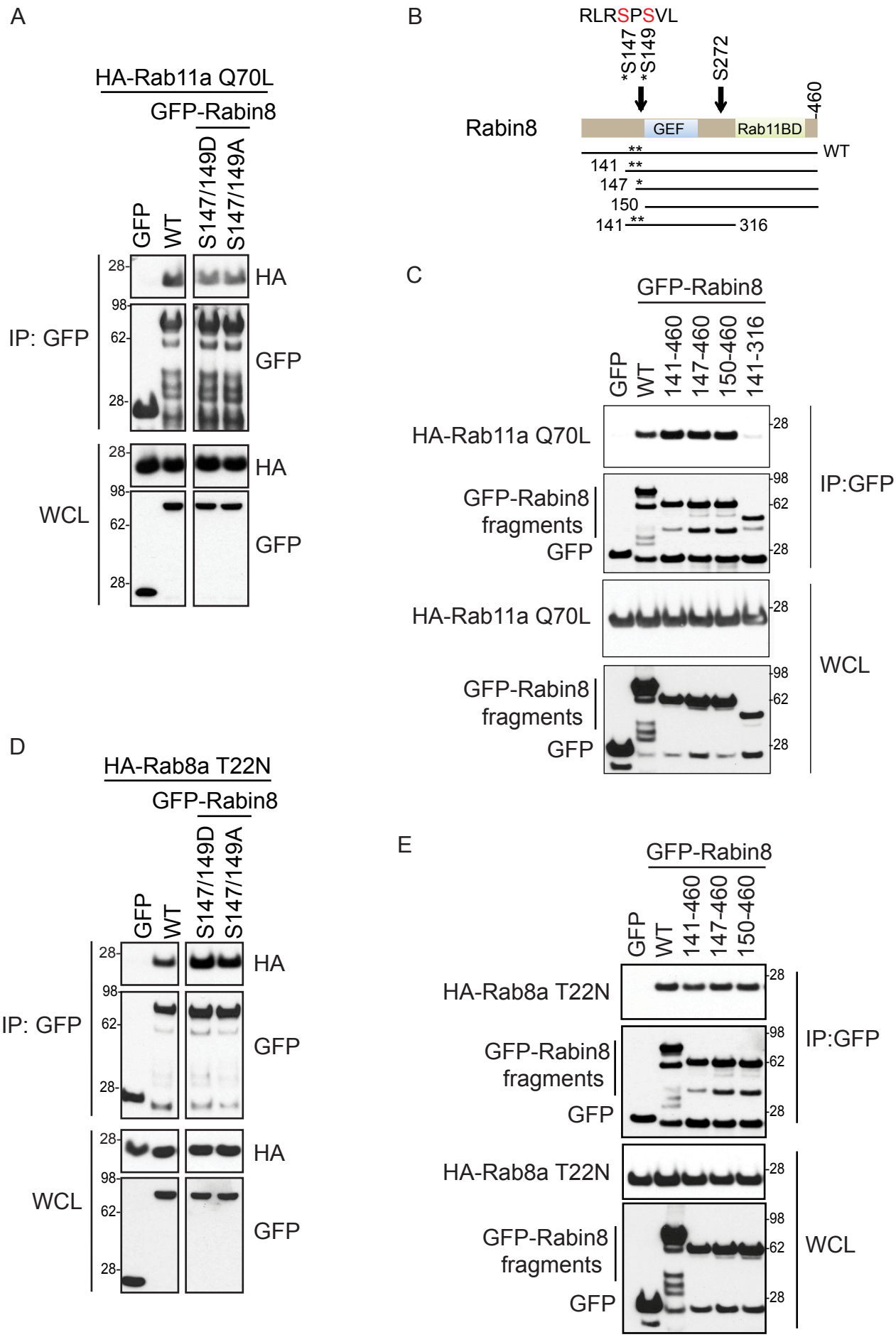
A
HA-Rab11a Q70L
GFP-Rabin8
GFP
WT
S147/149D
S147/149A
IP: GFP
HA
GFP
WCL
HA
GFP
28
98
62
28
B
RLRSPSVL
*S147
*S149
S272
Rabin8
GEF
Rab11BD
460
WT
141
147
150
316
C
GFP-Rabin8
GFP
WT
141-460
147-460
150-460
141-316
HA-Rab11a Q70L
GFP-Rabin8 fragments
GFP
IP:GFP
WCL
D
HA-Rab8a T22N
E

Figure S5

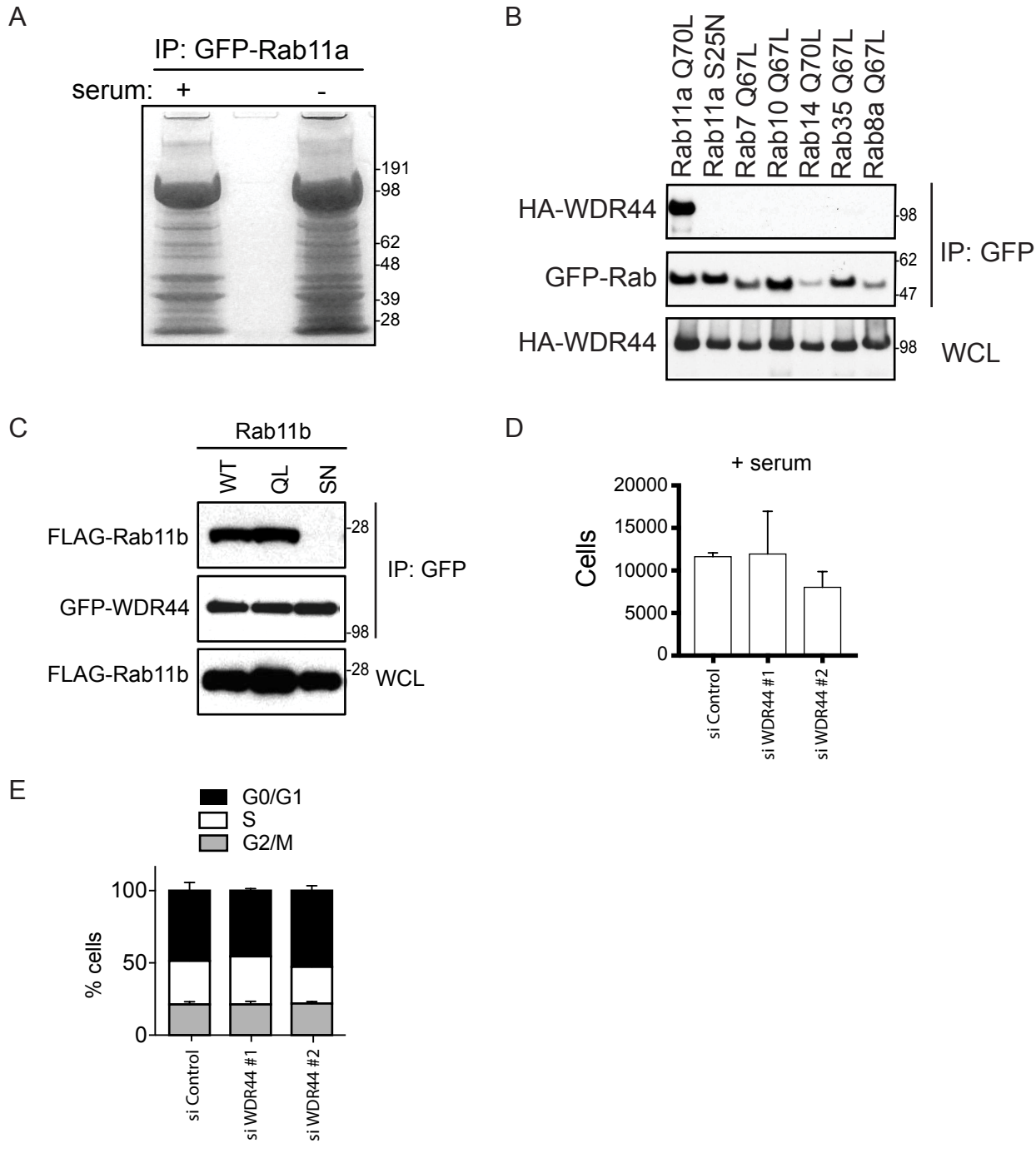
A
IP: GFP-Rab11a
serum: + -
191
98
62
48
39
28
B
Rab11a Q70L
Rab11a S25N
Rab7 Q67L
Rab10 Q67L
Rab14 Q70L
Rab35 Q67L
Rab8a Q67L
HA-WDR44
GFP-Rab
HA-WDR44
98
62
47
98
IP: GFP
WCL
C
Rab11b
WT
QL
SN
FLAG-Rab11b
GFP-WDR44
FLAG-Rab11b
28
98
28
IP: GFP
WCL
D
+ serum
Cells
20000
15000
10000
5000
0
si Control
si WDR44 #1
si WDR44 #2
E
G0/G1
S
G2/M
% cells
100
50
0
si Control
si WDR44 #1
si WDR44 #2

Figure S6

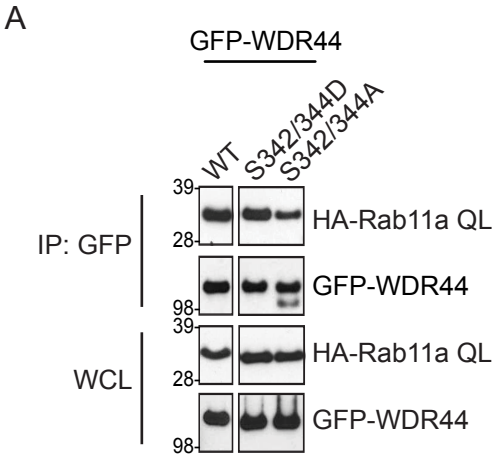
A
GFP-WDR44
WT
S342/344D
S342/344A
39
28
98
IP: GFP
HA-Rab11a QL
GFP-WDR44
39
28
98
WCL
HA-Rab11a QL
GFP-WDR44

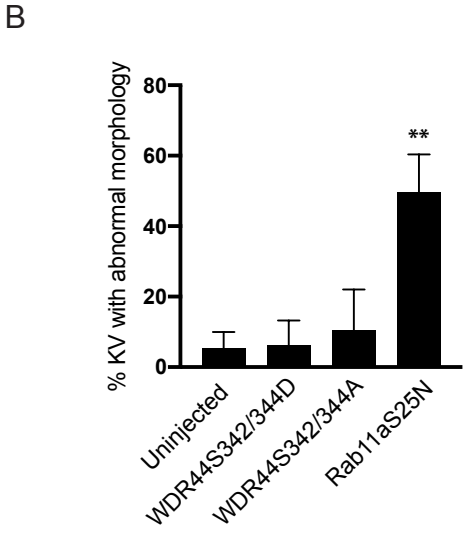
B
% KV with abnormal morphology
80
60
40
20
0
**
Uninjected
WDR44S342/344D
WDR44S342/344A
Rab11aS25N

Figure S7

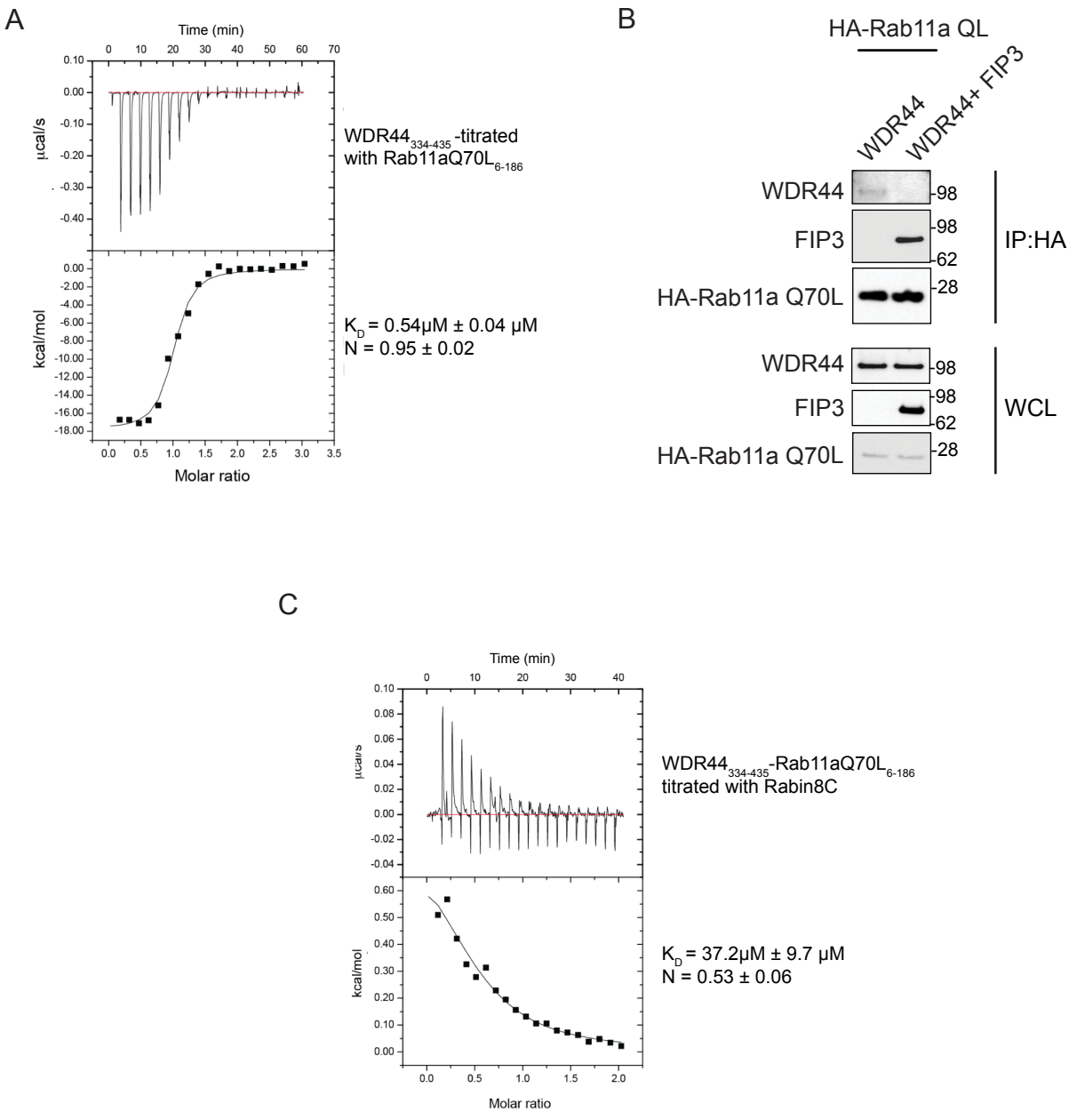
A
Time (min)
µcal/s
kcal/mol
Molar ratio
WDR44334-435-titrated
with Rab11aQ70L6-186
KD = 0.54µM ± 0.04 µM
N = 0.95 ± 0.02
B
HA-Rab11a QL
WDR44
WDR44+ FIP3
WDR44
FIP3
HA-Rab11a Q70L
IP:HA
WCL
98
62
28
C
Time (min)
kcal/mol
Molar ratio
WDR44334-435-Rab11aQ70L6-186
titrated with Rabin8C
KD = 37.2µM ± 9.7 µM
N = 0.53 ± 0.06